This is a repository copy of *Visualization study on the heat and mass transfer in the evaporator-compensation chamber of a loop heat pipe*.

White Rose Research Online URL for this paper:
http://eprints.whiterose.ac.uk/158028/

Version: Accepted Version

Visualization study on the heat and mass transfer in the evaporator-compensation chamber of a loop heat pipe

Qidong Zhang, Guiping Lin, Xiaobin Shen*, Lizhan Bai*, Dongsheng Wen

Laboratory of Fundamental Science on Ergonomics and Environmental Control, School of Aeronautic Science and Engineering, Beihang University, Beijing 100191, PR China

Abstract

To visually analyze the flow and heat transfer characteristics of the working fluid in a loop heat pipe (LHP), the evaporator-compensation chamber (CC) was designed as a half-sectioned cylindrical structure sealed with a glass window. Using acetone as the working fluid, visualization experiments were performed under different heat loads and tilt angles. The vapor-liquid distribution in the evaporator-CC coupling structure and the temperature variation characteristics of the LHP system were investigated at three tilt angles of the evaporator-CC coupling structure. According to the experimental results including the startup and steady-state operation, some important conclusions have been drawn as summarized below: 1) with the subcooled liquid outflow from the bayonet tube, the vapor-liquid interface in the evaporator-CC coupling structure rises when the heat load is applied to the evaporator; 2) the bubble generation inside the porous wick becomes more intense with an increased heat load, and there are various bubble movement patterns at different tilt angles; 3) the temperature fluctuation of the LHP system is closely related to the oscillation of the vapor-liquid interface in the evaporator core.

Keywords: loop heat pipe, evaporator, tilt angle, visualization, vapor-liquid interface

---

* Corresponding authors. Tel.: +86 10 8233 8600; Fax: +86 10 8233 8600

E-mail addresses: shenxiaobin@buaa.edu.cn (X. Shen); bailizhan@buaa.edu.cn (L. Bai)

1. Introduction

Loop heat pipe (LHP) is a two-phase heat transfer device that uses the capillary pressure to circulate the working fluid, and no external power is needed [1]. Compared with other heat transfer devices, an LHP has a variety of advantages such as high heat transport capability over long distances, high-precision temperature control, strong antigravity capability, compact design, convenient installation and passive operation. Consequently, the LHP has been identified by the aerospace engineers as the core component for future spacecraft thermal control systems [2-4].

In an LHP system, the evaporator plays an important role in enhancing the heat transport capability. The evaporator performance is closely related to the location of the compensation chamber (CC) and the path of the working liquid supply. There are two types of evaporator shapes: flat and cylindrical. Accordingly, there are two different evaporator and CC structures. To obtain more experimental data and more clearly study the mechanism in different evaporator structures, many researchers have conducted visual experiments on the LHPs. Basha [5] conducted visual experiments on a flat evaporator in an open-loop configuration to study bubble formation under different heat loads. Odagiri [6] used microscopic infrared thermography to record the visualization results of the thermal fluid behavior under different wicks with different materials and pore radii, and achieved a better polytetrafluoroethylene (PTFE) wick with less heat leak. For an LHP with cylindrical evaporator, Okamoto and Hatakenaka [7, 8] conducted visual experiments to study the vaporization phenomena in the evaporators with and without neutron radiography. Suh [9] visualized a porous wick for further analysis and focused on the effect of the spatial placement angle on the LHP. A visual experiment was conducted on the transparent micro-LHP with a flat porous silicon structure, and the thermodynamics inside the evaporator including vapor generation, nucleate boiling, evaporation, drying, and pressure oscillation were studied during steady-state operation. In addition to the visual investigations of the experimental components for clarifying the characteristics of an LHP, the influence of the working liquids was also analyzed.

Lin [10] conducted visual observation on the CC and condenser of a dual-compensation chamber loop heat pipe (DCC-LHP). The start-up and steady-state characteristics of the DCC-LHP were analyzed for different tilt angles between the evaporator and the CC. Instability was observed in the experiment and explained based on the results of the visual experiment. Visual experiments of the DCC-LHP for an aircraft anti-icing system were also conducted by Chang [11]. The start-up and operating characteristics of the DCC-LHP were studied, and the liquid surface changes in the two CCs were analyzed through glass windows under different angles of attack.

However, these studies focused on the visual evaporator or visual CC without an integrated structure. In an LHP system, an evaporator-CC coupling structure is widely used because this structural form can make the LHP system more compact and allow it to start up without preconditioning. Moreover, the heat transfer limit of the LHP can be enhanced because of the evaporator core in the wick. However, with the evaporator-CC coupling structure, unfavorable phenomena occur and affect system operation; these

phenomena include slow start-up due to the heat leak from the evaporator to the CC [12, 13], increase in the operating temperature, operation failure [14, 15], working fluid reverse flow and temperature fluctuation in the LHP, which affects the normal operation of the system [16, 17]. During ground operation, the tilt angles of the coupling structure directly determine the vapor-liquid distribution in the coupling structure and affect the heat leak from the evaporator to the CC [18]. According to its function, the evaporator-CC structure is equivalent to a set of temperature feedback system with an extremely complex internal heat and mass transfer mechanism. Therefore, it remains a difficult problem in this field.

Currently, visualization studies of LHPs focus mainly on the liquid lines, CC and flat LHP. However, to the best of the authors' knowledge, in-depth explorations to visualize the widely used cylindrical evaporator-CC coupling structure have not yet been performed. Because the cylindrical evaporator LHP has a high requirement for the match between the porous wick and the evaporator shell, in the visualization of the coupling structure, both the processing technology and sealing performance present challenges. This paper adopted a half-slice method to design, process, and assemble a cylindrical evaporator-CC coupling structure to observe the internal two-phase flow state in the coupling structure. Using visual designs to track the vapor-liquid interface, we studied the variation for the vapor-liquid distribution and working fluid flow in the LHP at three tilt angles: horizontal attitude, the CC at a higher position, and the evaporator at a higher position. Meanwhile, the heat and mass transfer characteristics of the LHP during the start-up and heat load increase were analyzed with the measured temperature curves. This visual method enables one to observe bubble generation/collapse and variations in the vapor-liquid interface inside the evaporator-CC structure during the start-up and transient process. Moreover, it provides an effective method to learn the influence mechanism of the heat leak and vapor-liquid interface fluctuations on the thermal characteristics of the LHP system.

2. Experimental system

2.1 Component design

In this paper, the traditional cylindrical evaporator-CC coupling structure was half-sectioned, and a quartz glass window was applied to visualize the internal vapor-liquid interface distribution and change. The overall design and assembly scheme of the visual experimental structure are shown in Fig. 1(a). Stainless steel was utilized as the shell material for the integrated design of the evaporator and CC to reduce the axial heat leak, and the outer wall surface of the shell connection was thinned to further decrease the heat conduction, as shown in Fig. 1(b). The half-sectioned porous wick was placed inside the evaporator shell, and the half-section end face was flush with the housing seal groove. For a good sealing effect, an EPDM gasket was evenly pressed to prevent the vapor leak from the vapor channels to the evaporator core. The quartz glass window was located on the sealing gasket to visually observe the evaporator-CC coupling structure. The pressing force on the glass was transmitted through the Teflon mat to ensure a uniform force on the window. The lightweight aluminum flange and stainless-steel shell were sealed by hexagon socket bolts to ensure that the working fluid in the

LHP was isolated from the external environment. Since the evaporator was relatively small and the reservoir volume of CC was large enough, the secondary wick was not used.

The key point and main difficulty for the visualization experiment are the porous wick processing and assembly. Because of its porous structure, the wick acts as a capillary pump to drive the circulation of the working fluid in the LHP. The preliminary molding of the porous wick was completed by pressing and sintering micron-sized nickel powders. Then, a central hole was drilled through the brittle porous medium to form the evaporator core (a liquid core). The outer dimensions of the porous wick were ensured by precision turning. Afterwards, threads (depth 0.2 mm; width 0.3 mm; angle 60°) were lathed, and vapor channels with 0.8 mm width and 0.8 mm height were milled. Finally, the cylinder was milled along its central surface to obtain a half section. Then, an interference fit of about 2–4 wires was formed between the section and the shell so that the section was closely fitted against the shell under the compaction force, and the thermal resistance was efficiently reduced. The specific structure of the processed porous wick is shown in Fig. 2.
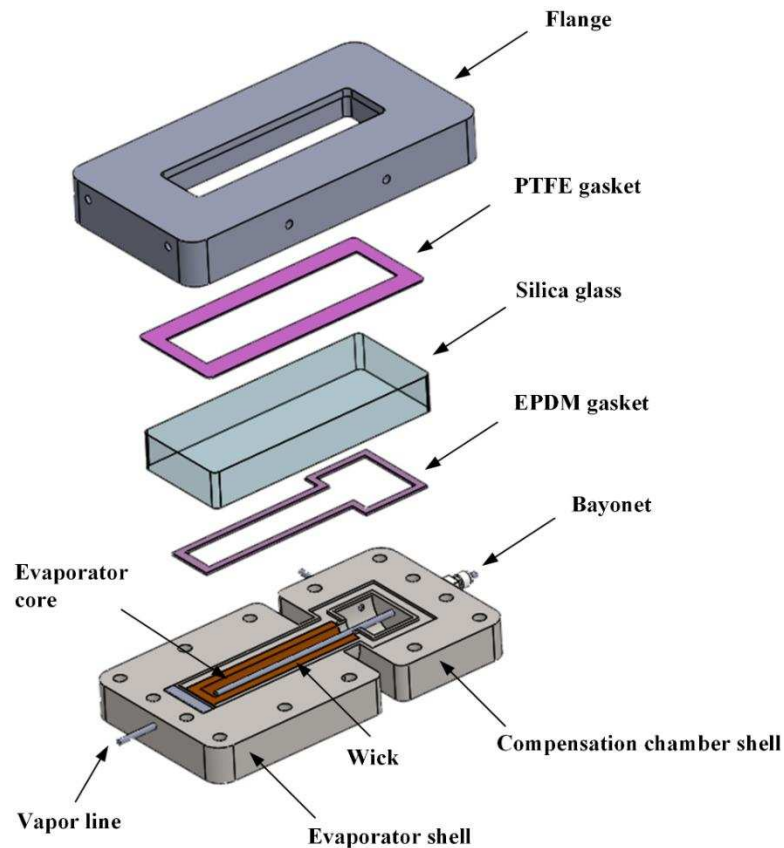
(a) Assembly diagram of the evaporator-compensation chamber
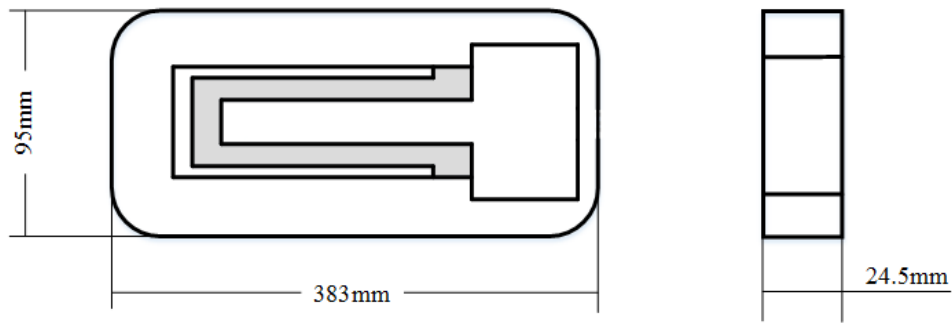
(b) Design of the evaporator-compensation chamber shell

Fig. 1 Schematic of the evaporator-compensation chamber coupling structure
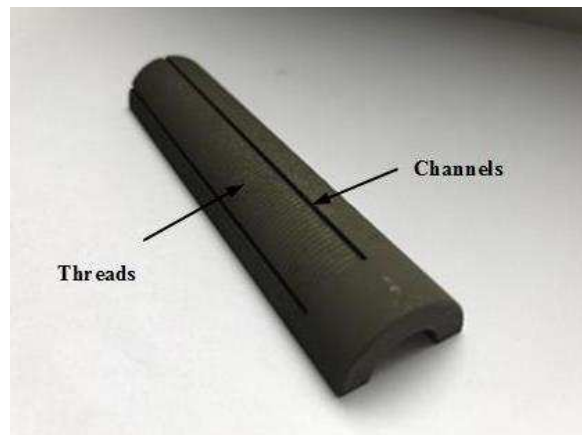
Fig. 2 Image of the porous wick

In addition, stainless-steel pipes with an outer diameter of 3 mm and an inner diameter of 2 mm were used in all transport lines of the LHP, including vapor lines, condenser lines, liquid lines, and the bayonet tube. Condenser lines were soldered to eight channels in the copper cold plate and cooled by a refrigerator at a constant cooling temperature of 10 °C. One end of the bayonet tube was connected to the liquid line, and the other end penetrated into the middle point of the evaporator core to ensure a better liquid supply and cooling for the porous wick. Considering the complexity of the experimental system, acetone, which is relatively stable, was selected as the working fluid. The relevant physical parameters of acetone is shown in Table 1. The basic parameters of the LHP components are shown in Table 2, where OD/ID represents the outer/inner diameters respectively.

Table 1 Physical properties of acetone

Temperature (K)	Vapor Pressure (MPa)	Liquid Density (kg/m³)	Vapor Density (kg/m³)	Surface Tension (mN/m)
300.00	0.033259	782.56	0.79564	22.731
310.00	0.050059	771.26	1.1678	21.364
320.00	0.073136	759.76	1.6678	20.014
330.00	0.10404	748.03	2.3251	18.683
340.00	0.14450	736.03	3.1730	17.371
350.00	0.19643	723.73	4.2492	16.079

360.00	0.26188	711.08	5.5969	14.808
370.00	0.34308	698.04	7.2655	13.56
380.00	0.44240	684.55	9.3127	12.334
390.00	0.56235	670.53	11.807	11.134
400.00	0.70559	655.92	14.830	9.9592

Table 2 Parameters of the experimental components

Component	Dimension
OD/ID×length of wick	Φ21/11×90 mm
Width/height×length of vapor groove	0.8/0.8×80 mm
Maximum pore diameter of wick	1.15 μm
Porosity of wick	50%
Permeability of wick	$1.3×10^{-14}\,m^2$
OD/ID×length of vapor line	Φ3/2×1150 mm
OD/ID×length of condenser line	Φ3/2×1950 mm
OD/ID×length of liquid line	Φ3/2×1090 mm
OD×length of evaporator core	Φ11×85 mm
OD/ID×length of CC	Φ35/31×250 mm

2.2 Experimental setup

As shown in Fig. 3, the entire visualization experimental system included an LHP to be tested, a temperature data acquisition system, a controllable power supply, a refrigerator, and a camera. A magnifier was mounted in front of the camera lens for better observations of the vapor-liquid flow in the evaporator-CC coupling structure. A 50 mm×100 mm polyimide heating film was attached to the outside of the evaporator shell to apply the heating power, and the heat load was controlled by adjusting the output voltage of the power supply. To reduce the effect of the ambient surroundings, air conditioning was used to maintain a constant room temperature of about 20 °C. To ensure clear photography, all the light sources in the room were turned off during the experiment except for a single point light source. To reduce the heat leak to the environment, all components of the loop except the observation window were wrapped with an adiabatic sponge.
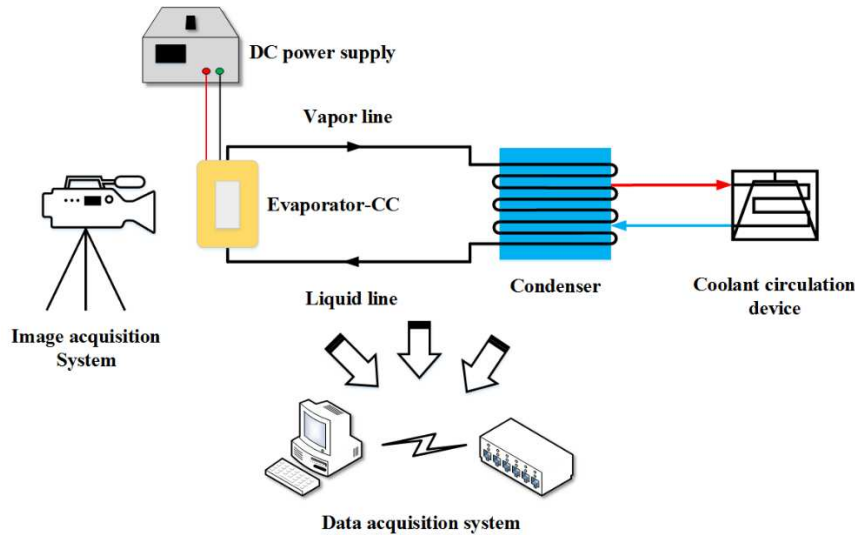
Fig. 3 Schematic of the visual experimental system

Type T thermocouples with an accuracy of about ±0.5 °C were adopted to measure the temperature change during the operation of the LHP system. The arrangement of the thermocouples in the system is shown in Fig. 4. There were 17 temperature measurement points in total, including two on the CC (Tc_1–Tc_2), three on the evaporator (Tc_3–Tc_5), two on the vapor line (Tc_6–Tc_7), eight on the condenser (Tc_8–Tc_{15}), and two on the liquid line (Tc_{16}–Tc_{17}). Because the heat capacity of the evaporator and CC was relatively large, the temperature measurements of the thermocouples on the wall of the shell were used only as qualitative references. All remaining thermocouples were located on the outer wall of the component to measure the temperature of the working fluid, which was considered equal to the outer wall temperature since the component wall was rather thin and insulated from the external surroundings.
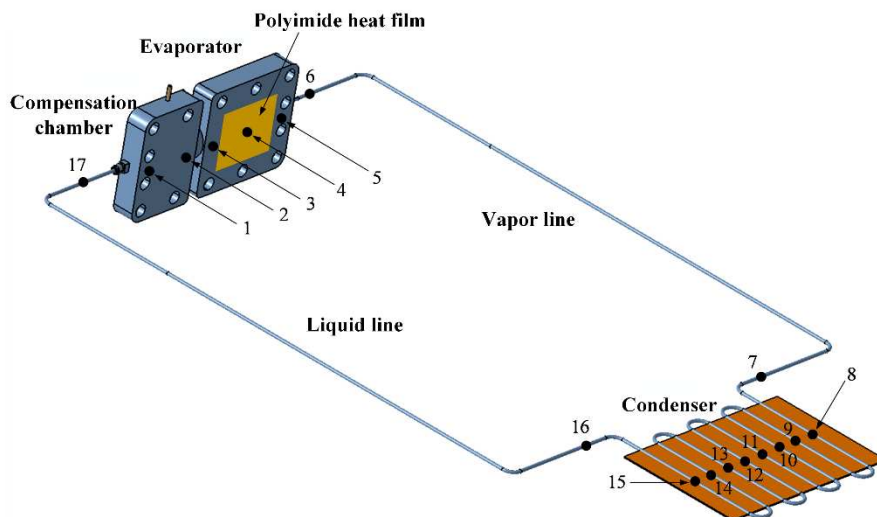
Fig. 4 Layout of the thermocouples

2.3 Experimental conditions

In this experiment, the well-established visual test facility was used to test the evaporator-CC coupling structure during the LHP start-up and operation at three tilt angles. The tilt angle β was defined as the angle between the axis of the evaporator and

the horizontal line. As shown in Fig. 5, three tilt angles in this experiment were $\beta= 0°$ for the horizontal attitude, $\beta= -15°$ for a lower position of the evaporator, and $\beta= 15°$ for a higher position of the evaporator. Considering the coupling effects of the tilt angle and heating power on the working fluid boiling condition inside the porous wick, different heat loads were applied for each evaporator position. Because of the low thermal conductance of the evaporator shell, the evaporator casing temperature could reach a very high value at a low heat load. Therefore, the experiments were carried out under a low heat load level. The specific experimental conditions are listed in Table 3 with a maximum heat load of 60 W.
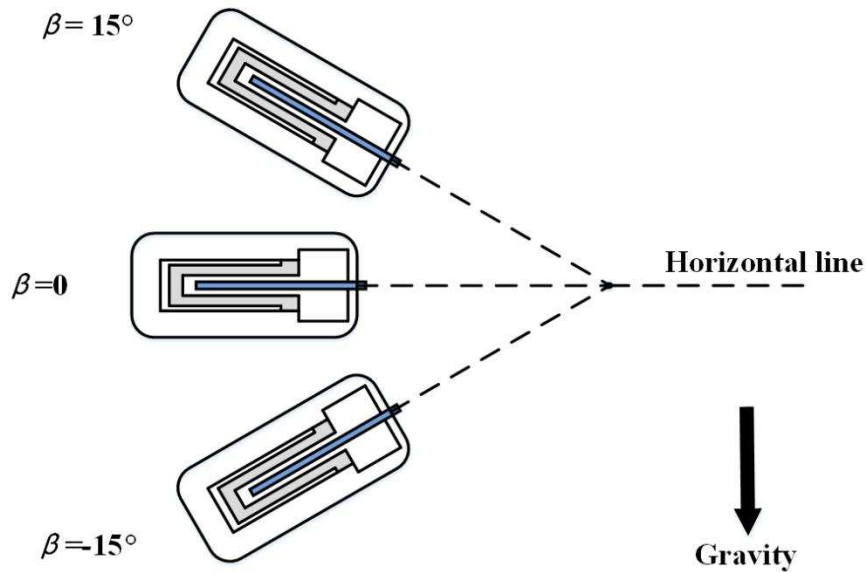
Fig. 5 Schematic of three attitude angles

Table 3 Experimental conditions

Tilt angle of evaporator $\beta/°$	Variation of heat load/W
0	20-40-60
-15	40-60
15	40-60

3. Experimental results and analysis

3.1 Start-up

3.1.1 Horizontal attitude ($\beta=0°$)

The distribution of the working fluid in the evaporator-CC coupling structure prior to applying the heat load is illustrated in Fig. 6, and a horizontal vapor-liquid interface below the bayonet tube was observed. After the level of the interface was maintained for a while, a heat load of 20 W was applied to the evaporator of the LHP. Then, the temperatures of the heating film Tc_4, evaporator Tc_3/Tc_5, and CC Tc_1/Tc_2 gradually increased, as shown in Fig. 7. The temperatures at the evaporator outlet Tc_6 and CC inlet Tc_{17} simultaneously slightly increased, while the temperatures of the condenser $Tc_8 - Tc_{15}$ barely changed. Thus, the temperature increases were clearly caused by

the heat conduction between the metal shell of the evaporator-CC coupling structure and the stainless-steel lines. After 50 min, the temperature at the evaporator outlet Tc_6 had not significantly increased, which indicated that no vapor flowed out of the evaporator. Meanwhile, the level of the vapor-liquid interface in the evaporator-CC barely changed from the initial state. Therefore, it was considered a start-up failure under a heat load of 20 W.
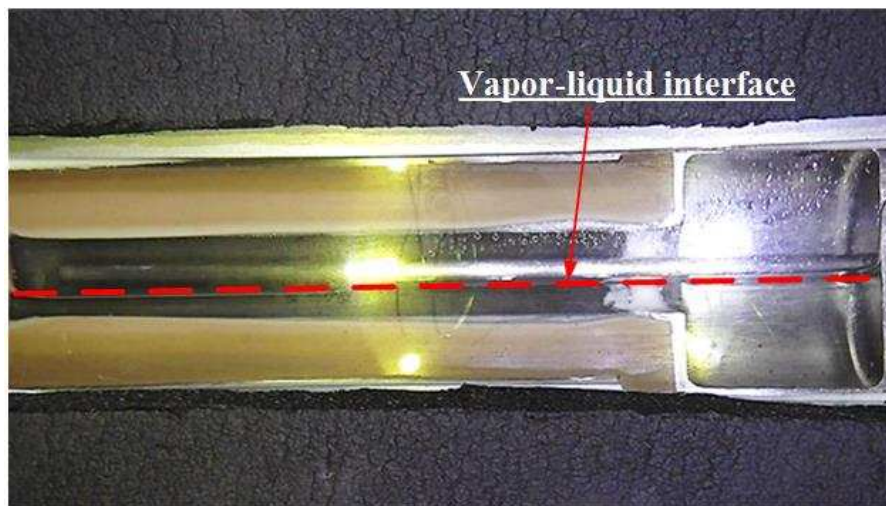
Fig. 6 Vapor-liquid distribution before power supply when β=0°
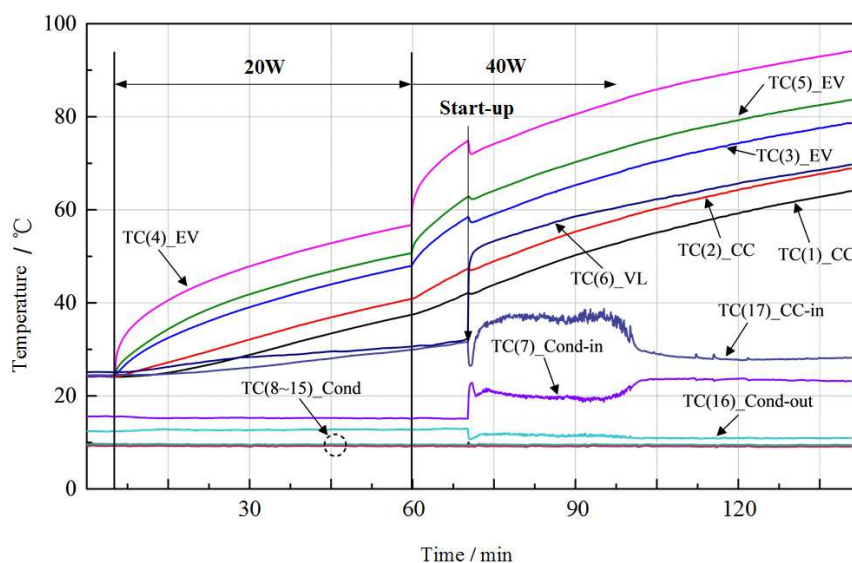
Fig. 7 Temperature curves at the heat loads of 20 W and 40 W

When we increased the heat load to 40 W, as shown in Fig. 7, the temperature at the evaporator outlet Tc_6 and condenser inlet Tc_7 increased rapidly after 10 min and 40 s, while the temperatures at the condenser outlet Tc_{16} and CC inlet Tc_{17} decreased. Hence, there was liquid working fluid flowing from the condenser into the CC, and the LHP successfully started up. Meanwhile, liquid outflow was observed from the bayonet tube outlet, and the working fluid flowed along the evaporator core to the CC. However, the temperature at the condenser inlet Tc_7 rapidly decreased after the increase at the start, while the temperature change at the CC inlet Tc_{17} was opposite. The high pressure caused by the working fluid boiling in the evaporator drove the vapor to flow

into the condenser, but the redistribution of the vapor and liquid inside the LHP was not completed. In addition, the vapor generation was insufficient to form a continuous flow and stable operation for the entire loop. As a consequence, the liquefaction pressure in the vapor line decreased, and the liquid refluxed in the condenser.

As the liquid working fluid continued flowing into the evaporator-CC coupling structure, the vapor-liquid interface level gradually rose. Vapor generation on the inner surface of the wick and the surface tension of the liquid working fluid caused slug bubbles with an unstable liquid inflow to form in the upper part of the evaporator core near the bayonet tube outlet, as shown in Fig. 8. The processes of bubble generation, flow and merge were accompanied by pressure oscillations and heat exchange, which affected the flow and heat transfer of the entire LHP system and resulted in the continuous slight temperature fluctuation at the CC inlet Tc_{17} and condenser outlet Tc_{16}.
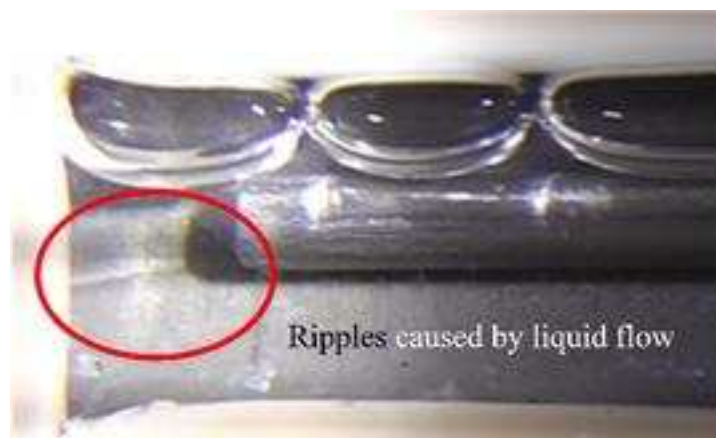
(a) Liquid outflow from the bayonet tube and bubbles
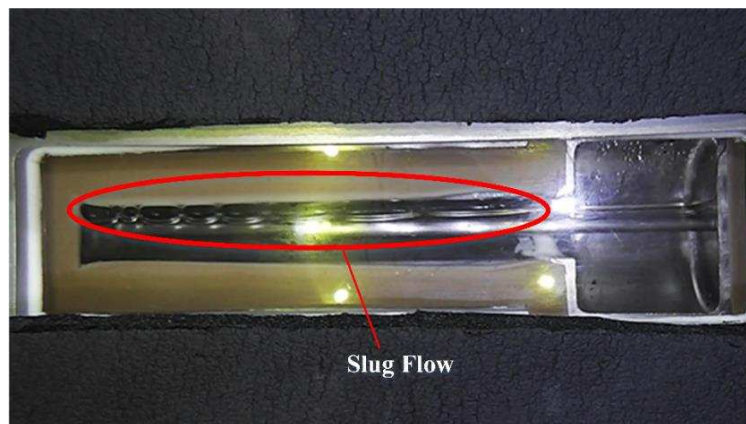
(b) Bubble flow in the evaporator core

Fig. 8 Flow in the evaporator-compensation chamber coupling structure

After applying 40 W of power for 100 min, the temperatures at Tc_7 and Tc_{17} began to stabilize. In Fig. 9, the visual window shows that the vapor-liquid distribution in the evaporator-CC coupling structure was stable, and the liquid level was above the bayonet tube, although bubbles continued to be generated on the wick inner surface. In addition, the liquid inflow was steady, and there was no large-scale bubble generation and no fluctuation in the vapor-liquid interface. When the redistribution of the working

fluid in the LHP was basically completed, the heat leak from the evaporator to the CC was balanced, and the working temperature became stable.
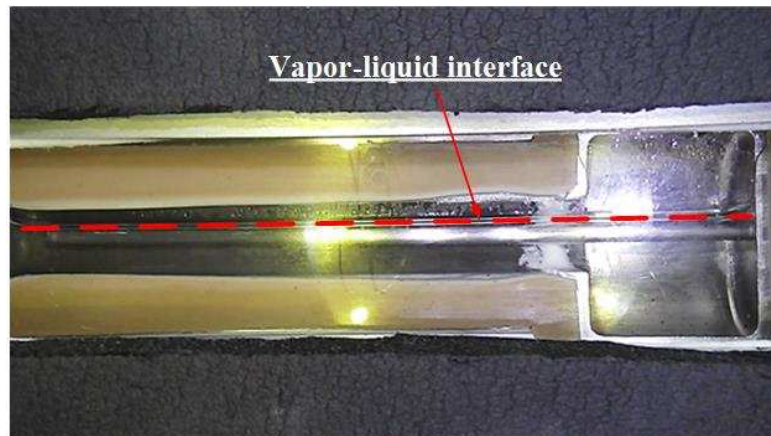
Fig. 9 Vapor-liquid distribution at 40 W

3.1.2   Evaporator at a lower position ($\beta=-15°$)

When the CC was placed at a higher position than the evaporator, due to the action of gravity, the working liquid was concentrated mainly in the evaporator core, and only a small amount of working fluid was in the CC, as shown in Fig. 10. To successfully start up the LHP, the experiment was began with a heat load of 40 W. Fig. 11 shows that the temperature of the evaporator shell immediately increased. After 2 min and 30 s, the temperature at the evaporator outlet Tc_6 sharply increased, which indicates the vapor outflow from the evaporator. Simultaneously, the level of the vapor-liquid interface in the evaporator-CC coupling structure rose. Fig. 12 shows that, with a continuous increase in liquid level, the evaporator core was almost filled with the working fluid, and the liquid proportion in the CC increased.

At this tilt angle, the subcooled liquid that flowed out of the bayonet tube cooled the evaporator core around the outlet. Consequently, no bubbles were generated on the inner surface of the nearby wick. However, due to the relatively high wall temperature compared to the liquid temperature, boiling occurred away from the bayonet tube outlet on the inner wick surface, and many bubbles formed in the evaporator core originally filled by the working liquid (Fig. 13). Driven by the buoyancy force, these bubbles aggregated into larger ones and flowed to the CC with the heat flux transfer.

Fig. 10 Vapor-liquid distribution before the power supply
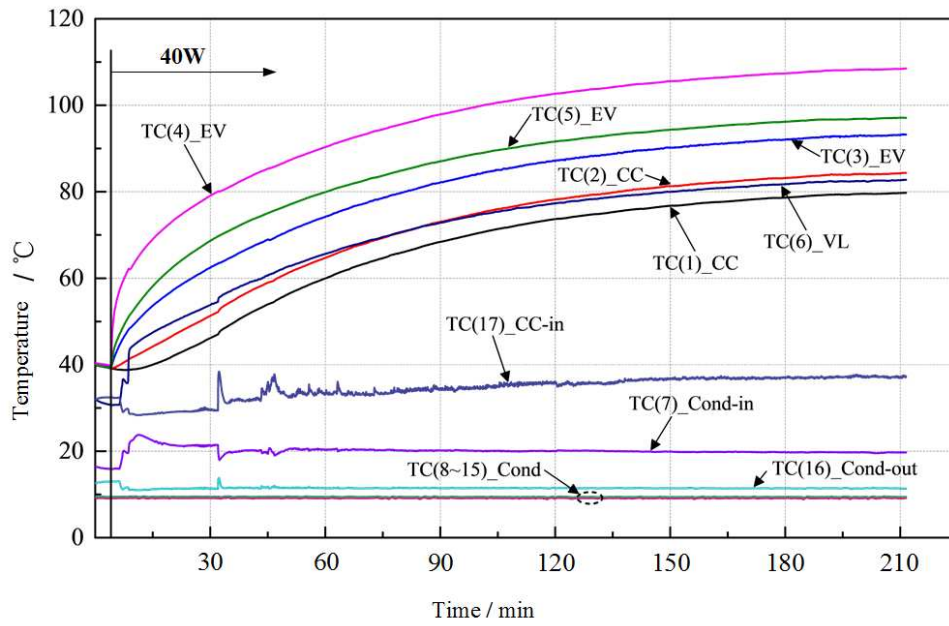
Fig. 11 Temperature variation curves at 40 W when *β*=−15°
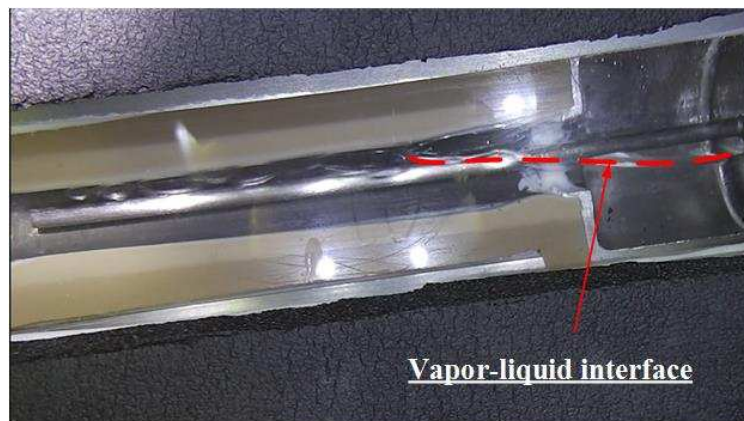
Fig. 12 Vapor-liquid distribution at 40 W
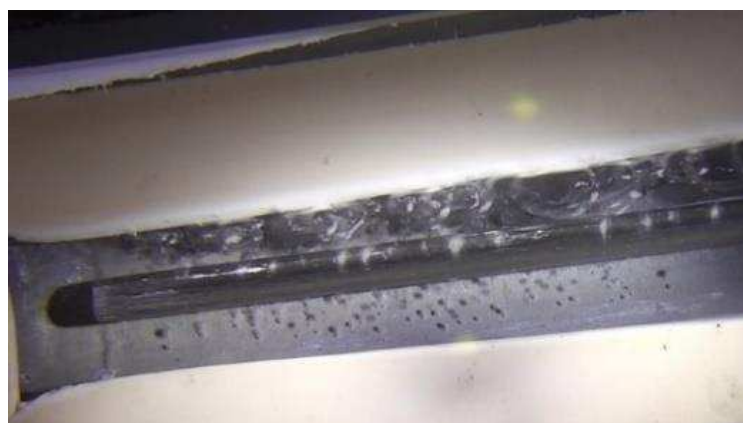
Fig. 13 Bubble aggregation in the evaporator core

The temperature of the system during start-up at this tilt angle was more stable than it was at the horizontal attitude because, when the evaporator was placed at a lower position (*β*= −15°), the working liquid for the evaporator-CC coupling structure

accumulated in the evaporator core, which ensured continuous boiling and evaporation in the vapor channels of the wick. In addition, since the bayonet tube outlet was sealed by the working liquid, the fluctuation in the vapor-liquid interface slightly affected the working fluid flow in the LHP. Therefore, the phenomenon of backward flow was not obvious.

3.1.3   Evaporator at a higher position (β=15°)

The vapor-liquid distribution inside the evaporator-CC coupling structure before applying a heat load at 15 degrees (β=15°) is shown in Fig. 14. Most of the working liquid accumulated in the CC, and only a small amount was in the evaporator core, which created a vapor zone around the bayonet tube outlet.

After a heat load of 40 W was applied for a time, there was liquid outflow from the bayonet tube. Due to the effect of gravity and the surface adhesion force, the liquid flowed directly along the outer wall of the bayonet tube to the CC without staying in the evaporator core, as shown in Fig. 15. With more liquid entering, the vapor-liquid interface in the evaporator-CC coupling structure gradually increased. Fig. 16 shows that the CC was almost full of working liquid, and the amount of working liquid in the evaporator core also increased. The bending of the vapor-liquid interface in Fig. 16 was caused by the wettability of the solid wall. In addition, bubbles formed on the inner wick surface and flowed to the evaporator core instead of the CC. Therefore, the phase-change heat leak caused by the mass transfer of bubble movement was limited. The bubble generation position and production rate gradually increased for the heat load applied and coupled with the movement of the inflow liquid to result in a continuous fluctuation of the vapor-liquid level in the coupling structure, as shown in Fig. 17. Although the bayonet tube outlet was above the liquid level, the fluctuation in the vapor-liquid interface caused the pressure change in the upper vapor space, which also resulted in the temperature fluctuations.

In addition, Fig. 18 shows a discontinuous peak in the temperature at the CC inlet Tc_{17}. This phenomenon resulted from the backflow of the intermittent working fluid in the bayonet tube, which was caused by the bubble generation in the coupling structure; thus, the vapor pressure instantaneously increased. The bubble generation and its effect on the vapor-liquid interface and vapor pressure in the coupling structure are also observed in Fig. 17.
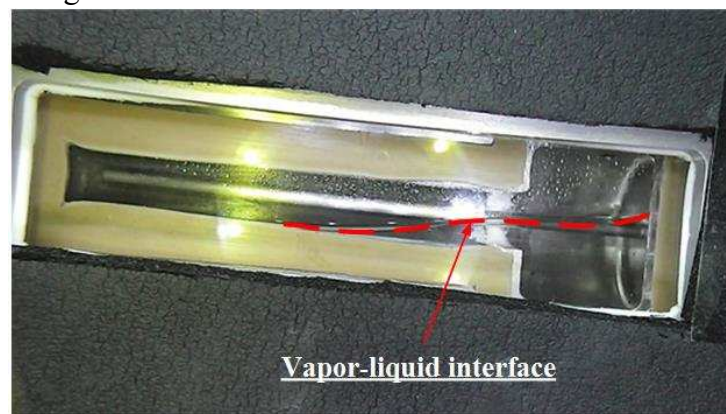
Fig. 14 Vapor-liquid distribution before applying power
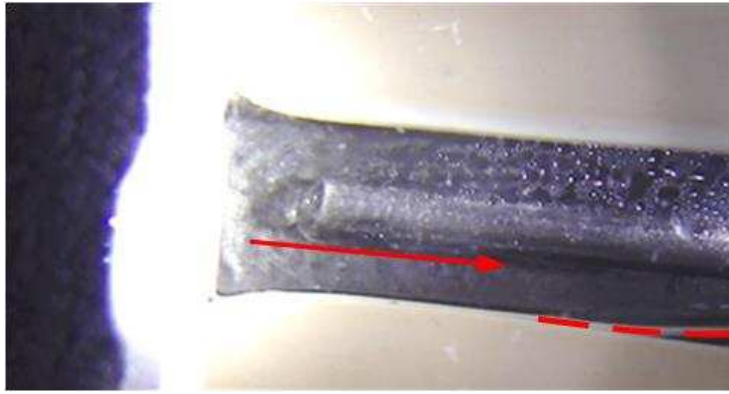
Fig. 15 Liquid outflow from the bayonet tube
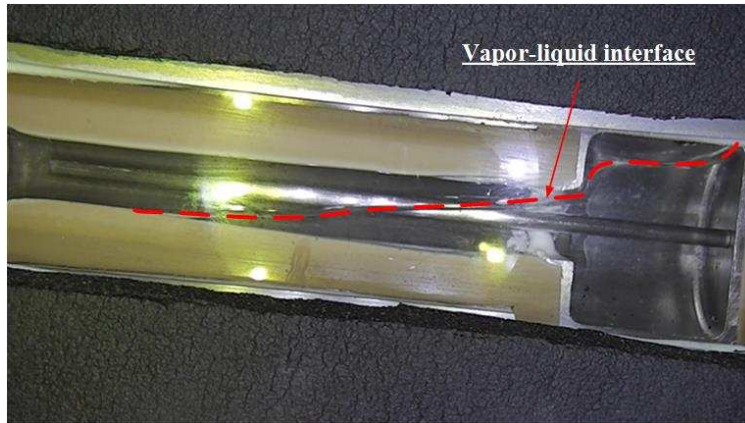
Fig. 16 Vapor-liquid distribution at a heat load of 40 W
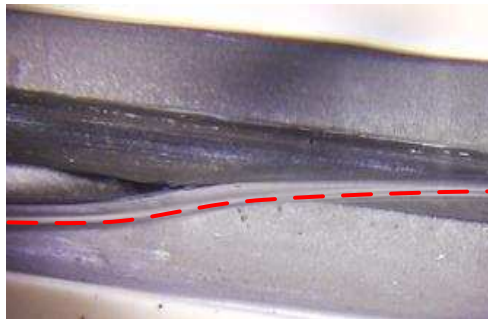
Fig. 17 Fluctuation of the vapor-liquid interface
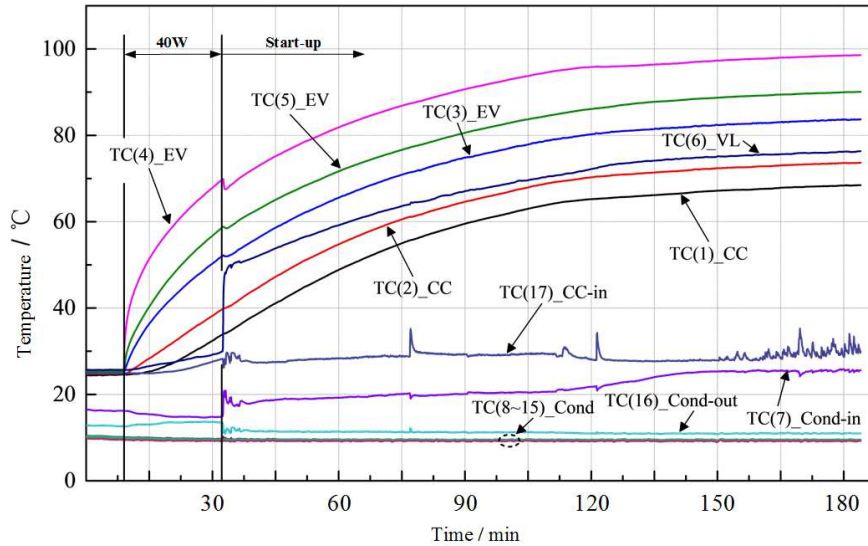
Fig. 18 Temperature variation curves at 40 W when *β*=15°

The start-up time of the LHP at this tilt angle was longer than that at *β*=−15° because the working liquid concentrated mainly in the CC and required a long path with extra driving force against gravity to reach the evaporation position. Consequently, the large pressure drop in the wick and the small flow rate hindered the start-up of the LHP and increased the start-up time of the system. The start-up state of the system at this tilt angle also had a more obvious temperature fluctuation than that at -15 degrees. When *β*=15°, the bayonet tube outlet was located within the vapor space of the coupling structure. Therefore, the working fluid flow in the LHP system was greatly affected by the pressure change in the structure, and the temperature fluctuated more significantly.

3.2 Power increment test

3.2.1   Horizontal attitude (*β*=0°)

Fig. 19 (a) shows that after we increased the power from 40 W to 60 W, the boiling was more intense on the inner surface of the wick, and bubbles were continuously formed on the inner surface of the wick. Because of the buoyancy, the bubbles moved upwards and merged in the upper part of the evaporator core. Fig. 19 (b) shows that, due to the fast bubble generation speed, the processes of gathering and merging were very violent. Driven by the vapor pressure and buoyancy, many bubbles flowed towards the CC and caused a large amount of heat leak from the evaporator to the CC and severe fluctuations in the vapor-liquid interface, as shown in Fig. 19 (c). When the heat load was maintained at 60 W, more liquid flowed into the evaporator-CC coupling structure, and so the liquid level was supposed to rise to spread across the entire evaporator core. However, Fig. 19 (c) shows that there was a vapor passage formed by the bubble accumulation in the upper part of the evaporator core, although the vapor-liquid interface rose in the evaporator-CC structure. The violent fluctuations in the pressure and the vapor-liquid interface in the coupling structure affected the working fluid flow in the LHP system. Therefore, a continuous redistribution of the working liquid occurred among the CC, evaporator core, and transfer lines. As shown in Fig. 20, the temperature at the CC inlet Tc_{17} experienced sharp fluctuations several times before

stabilizing.
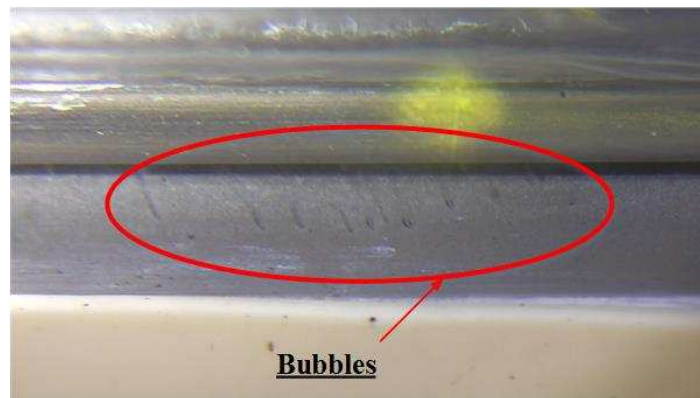
(a) Bubble generation

(b) Bubble movement and aggregation
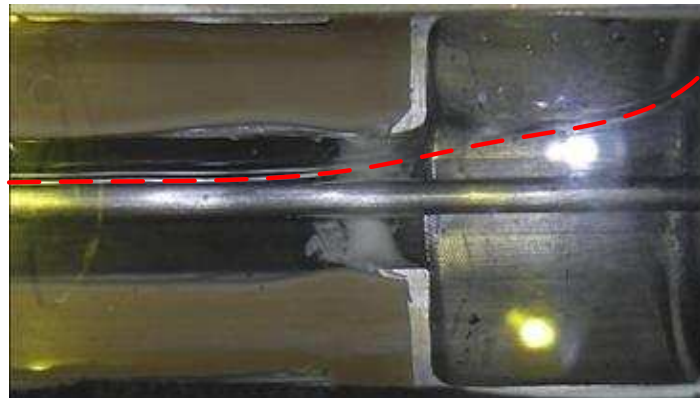
(c) Violent reactions on the liquid surface caused by the bubbles

Fig. 19 Bubble generation and movement at 60 W
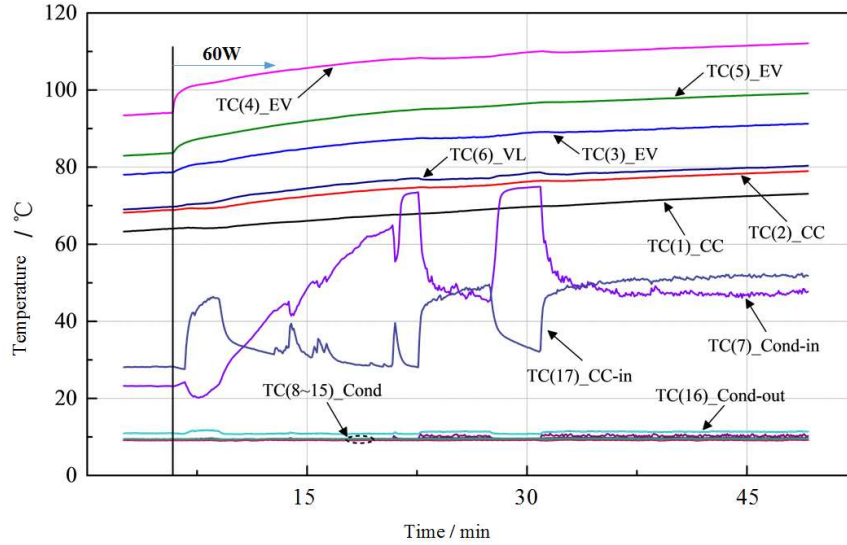
Fig. 20 Temperature variation curves at 60 W when *β*=0°

3.2.2　Evaporator at a lower position (*β*=-15°)

When the system reached a steady state at 40 W, the heat load was increased to 60 W at *β*=-15°. In Fig. 21, after a period, the temperature at the condenser inlet Tc_7 increased to approach the temperature at the evaporator outlet Tc_6, which indicates that the effect of condenser heat conduction was eliminated. The vapor-liquid interface in the evaporator-CC rose higher than the evaporator core, but the liquid working fluid did not fill the CC, as shown in Fig. 22. In addition, with a higher generation rate, bubbles were formed at more places on the inner surface of the porous wick under this heat load (Fig. 23). Bubbles also aggregated in the evaporator core and flowed to the CC, but the actions were more violent. The bubbles condensed in the CC with the heat leak to the CC. In addition, there were no bubbles around the bayonet tube outlet, which resulted in a small pressure fluctuation and a smooth temperature curve, as shown in Fig. 21.
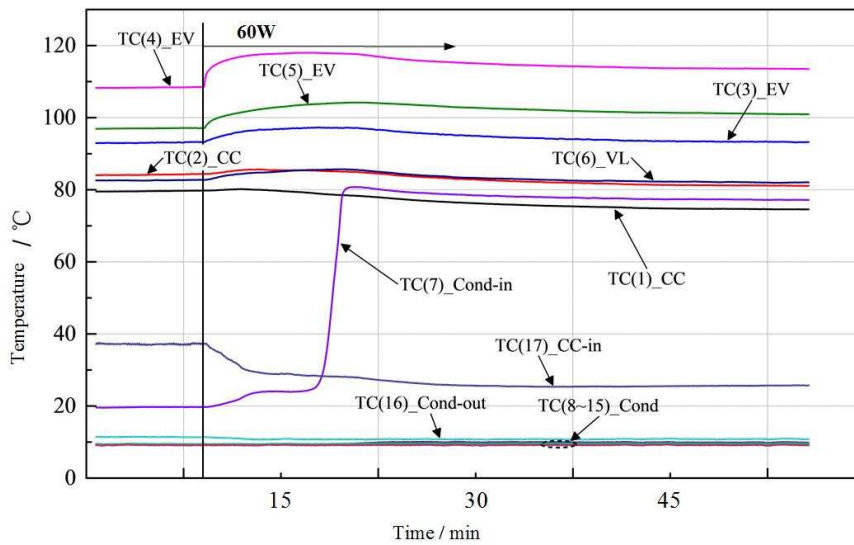
Fig. 21 Temperature variation curves at 60 W when *β*=−15°
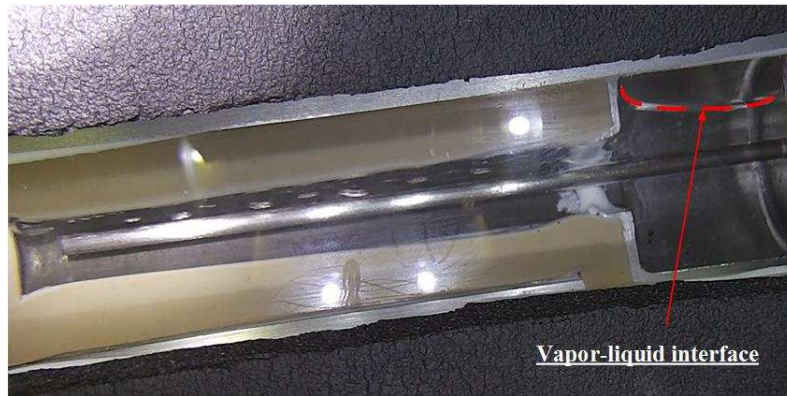
Fig. 22 Vapor-liquid interface distribution at 60 W

Fig. 23 Bubble aggregation in the evaporator core

Compared with the results in the horizontal attitude, the operating temperature of the system was more stable because, due to the liquid seal formed by the working liquid concentrated in the evaporator core, the vapor-liquid interface fluctuation in the coupling structure had less of an impact on the working fluid flow in the LHP. In addition, compared with the results at 40 W of power, the vapor-liquid interface level was higher in the evaporator-CC coupling structure, and the bayonet tube outlet near the bottom of the liquid was less affected by the interface fluctuation.

3.2.3　Evaporator at a higher position (β=15°)

When the heat load power increased to 60 W and β=-15°, the temperature variation curves are as shown in Fig. 24. Shortly after the increase in power, temperature fluctuations with a period of approximately 60 s occurred at almost all temperature measurement points, among which the temperatures of the CC inlet Tc_{17} and condenser inlet Tc_7 most violently fluctuated. Those temperature fluctuations were caused by the overall oscillation of the working fluid in the LHP, which will be described in detail in section 3.3.
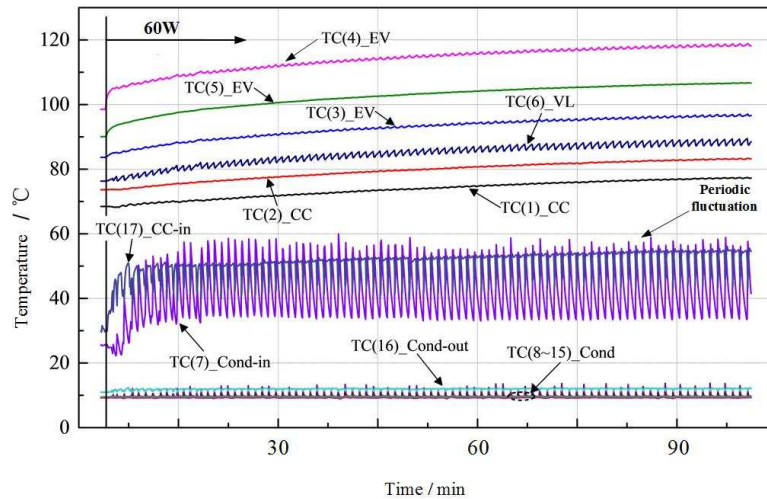
Fig. 24 Temperature variation curves at 60 W when *β*=15°

It was observed through the window that the liquid level rose at 60 W, and the vapor-liquid interface in the coupling structure periodically changed. In addition, the liquid working fluid was intermittently jetted out from the bayonet tube outlet. Meanwhile, the position and generation rate of the bubbles in the evaporator core increased, and violent fluctuations in the vapor-liquid interface were observed in the coupling structure, as shown in Fig. 25. Further observations reveal that, when the liquid working fluid entered the evaporator core from the bayonet tube, many small bubbles were formed on the inner wick surface, mainly due to the pressure oscillations with the vapor-liquid interface.

Fig. 25 Fluctuations in the liquid surface caused by the bubbles and subcooled liquid injection

3.3 Fluctuation phenomena

The experimental results show that the fluctuations in the system temperature resulted from the fluctuations in the vapor-liquid interface and system pressure, which were caused by the bubble generation and movement in the evaporator-CC coupling structure. Specifically, at the horizontal attitude (*β*=0°), the effect of the vapor-liquid interface and pressure oscillations was moderate, and the fluctuations of the operating temperature were higher than those at -15 degrees but lower than that at 15 degrees. When the evaporator was below the CC (*β*=-15°), the bayonet tube outlet was located at the bottom of the liquid zone far from the vapor-liquid interface, and there was no bubble generation. Therefore, the flow and vapor-liquid distribution in the LHP was slightly affected by the oscillations in the coupling structure. When the evaporator was

higher than the CC (β=15°), and most of the working fluid accumulated in the CC, unstable evaporations tended to occur due to the higher fluid supply resistance in the evaporator. Meanwhile, since the bayonet tube outlet was located in the vapor zone, the pressure oscillations caused by the fluctuation of the vapor-liquid interface acted directly on the outflowing subcooled liquid. Consequently, both mass flow and working fluid distribution in the LHP system were affected, and the temperature fluctuations were significant. Especially at 60 W, periodic injections of the working liquid in the coupling structure and violent temperature fluctuations in the entire system were observed.

To study the cause of the significant temperature fluctuations when β=15°, analysis was performed in terms of a single temperature fluctuation period in Fig. 24. Distributions of the vapor-liquid interface in the evaporator-CC coupling structure are shown at different times in Fig. 26, where t=0 s was defined as the time when the liquid content in the coupling structure reached its maximum value. Since the evaporator was at a higher position, a liquid seal was formed between the CC and the evaporator, and the liquid level was the highest with a small amount of vapor in the CC at t=0 s. When the LHP was in operation, vapor and bubbles continuously formed on the inner wick surface and accumulated in the evaporator core under the action of buoyancy. With time, the volume and pressure of the vapor space in the evaporator core gradually increased, which prevented the liquid from outflowing from the bayonet tube and the temperature from rising. In Fig. 26(b), the vapor space in the evaporator core increased, whereas that in the CC shrank due to condensation at t=15 s. The vapor space in the evaporator core approached the maximum value at t=43 s, when the liquid seal remained. At this moment, because of the condensation in the CC, the pressure in the CC was lower, and the entire CC was filled with the liquid working fluid. When the vapor pressure in the evaporator core further increased, the vapor broke through the liquid seal and entered the CC at t=56 s, which caused violent fluctuations in the liquid level and abrupt changes in the pressure. Meanwhile, the vapor mixed with the cold liquid in the CC and condensed into the liquid; thus, the pressure in the evaporator core suddenly dropped. The pressure drop allowed the subcooled liquid to flow out through the bayonet tube and made the boiling in the wick more intense with a large number of small bubbles. At t=58 s, a subcooled liquid outflow continued from the bayonet tube, which cooled the evaporator core to reduce the temperature and pressure. The subcooled liquid continued to flow out until the vapor-liquid interface reached the highest position, and the circulation was completed.

| (a) t=0 s | (b) t=15 s |

<div align="center">(c) t=43 s   (d) t=56 s</div>
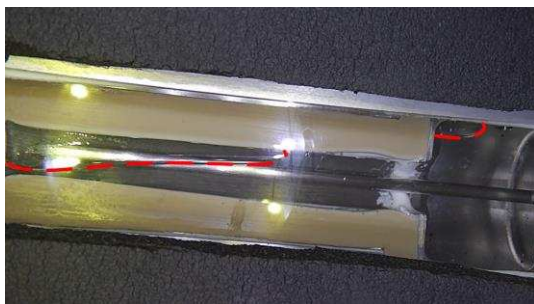
<div align="center">(e) t=58 s</div>
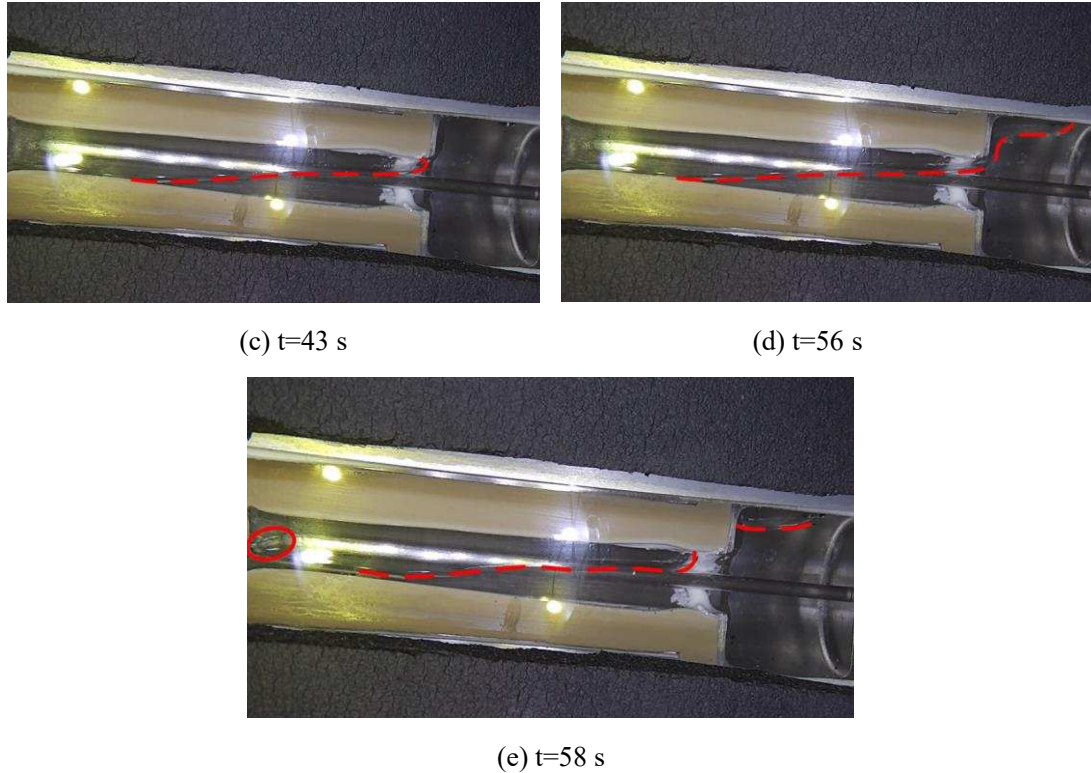
Fig. 26 Distributions of the vapor-liquid interface at different times

4. Conclusions

The flow and heat transfer characteristics of the working fluid in the evaporator-CC coupling structure of an LHP at three tilt angles were studied based on a visual experimental system. Because of the low evaporator conductance, the operating heat load was restricted to a small range from 0-60 W. According to the observational results and collected temperature data, the main conclusions are summarized as follows:

1) The vapor-liquid interface in the evaporator core at different tilt angles rises during the LHP start-up and heat load increase processes. Unsteady changes in the vapor-liquid interface in the coupling structure affect the operation of the LHP system and result in temperature fluctuations and working fluid redistributions.

2) Bubbles are generated on the inner surface of the wick and become more intense when the heat load increases. The bubbles merge and flow to various positions for different tilt angles with different heat leak characteristics.

3) The temperature fluctuations in the LHP are caused by oscillations in the vapor-liquid interface and the pressure in the evaporator-CC coupling structure. In particular, at a 15-degree tilt angle when the heat load was 60 W, a periodic oscillation of the vapor-liquid interface is clearly observed and analyzed in detail.

This work reports a preliminary study on the flow and heat transfer characteristics of the working fluid in the evaporator-CC coupling structure of an LHP by using the visualization method. Some interesting phenomena such as the periodic oscillation of the vapor-liquid interface in the evaporator core were observed and analyzed. The heat load applied to the evaporator was in a small range due to the low thermal conductance of the evaporator shell, which needs to be improved. In addition, the heat loss from the

glass window to the ambient is also a problem to be solved in future experiments.

5. Acknowledgment

References

[1] Y.F. Maydanik, Loop heat pipes, Applied Thermal Engineering. 25(2005) 635-657.

[2] G. Wang, D. Mishkinis, D. Nikanpour, Capillary heat loop technology: Space applications and recent Canadian activities, Applied Thermal Engineering. 28(2008) 284-303.

[3] M.T. Pauken, G. Birur, M. Nikitkin, F. Al-Khabbaz, Thermal performance evaluation of a small loop heat pipe for space applications, in: 33rd International Conference on Environmental Systems, 2003.

[4] L.L. Vasiliev, E.P. Beliyvskiy, A.P. Elchin, Y.M. Prochorov, V.M. Gulia, S.V. Zaletaev, R.M. Kopyatkevitsh, Experience of heat pipes application in spacecraft thermal control system, in: Proc. 5th Minsk Int. Seminar Heat Pipes, Heat Pumps, Refrigerators, 2003.

[5] M.S. Basha, L. Bansal, D. Sarma, S. Basu, P. Kumar, A. Ambirajan, Solar thermal power system augmented with LHP, Energy Procedia. 49(2014) 295-304.

[6] K. Odagiri, M. Nishikawara, H. Nagano, Microscale infrared observation of liquid-vapor phase change process on the surface of porous media for loop heat pipe, Journal of Electronics Cooling and Thermal Control. 6(2016) 33-41.

[7] R. Hatakenaka, A. Okamoto, Y. Mase, M. Murakami, H. Iikura, Visualization of internal fluid behavior in a miniature loop heat pipe using neutron radiography, in: 41st International Conference on Environmental Systems, 2011.

[8] A. Okamoto, R. Hatakenaka, Y. Mase, M. Murakami, Visualization of a loop heat pipe using neutron radiography, in: International Conference on Environmental Systems, 2013.

[9] J. Suh, D. Cytrynowicz, P. Medis, F.M. Gerner, H.T. Henderson, Flow visualization within the evaporator of planar loop heat pipe, AIP Conference Proceedings. 746(2005) 195-202.

[10] G. Lin, N. Li, L. Bai, D. Wen, Experimental investigation of a dual compensation chamber loop heat pipe, International Journal of Heat and Mass Transfer. 53(2010) 3231-3240.

[11] Y. Zhao, S. Chang, B. Yang, W. Zhang, M. Leng, Experimental study on the thermal performance of loop heat pipe for the aircraft anti-icing system, International Journal of Heat and Mass Transfer. 111(2017) 795-803.

[12] M.A. Chernysheva, Y.F. Maydanik, J.M. Ochterbeck, Heat transfer investigation in evaporator of loop heat pipe during startup, Journal of Thermophysics and Heat Transfer. 22(2012) 617-622.

[13] V.G. Pastukhov, Y.F. Maidanik, Y.G. Fershtater, Adaptation of loop heat pipes to zero-g conditions, Proceedings of Sixth European Symposium on Space Environmental Control Systems. 400(1997) 385-391.

[14] J. Ku, L. Ottenstein, P.R. Army, T. Warren, K.C. Mi, Investigation of low power operation in a loop heat pipe, in: 31st International Conference on Environmental Systems, 2001.

[15] D. Douglas, J. Ku, T. Kaya, Testing of the Geoscience Laser Altimeter System (GLAS) prototype loop heat pipe, in: 37th AIAA Aerospace Sciences Meeting and Exhibit, 1999.

[16] J. Ku, L. Ottenstein, M. Kobel, P. Rogers, T. Kaya, Temperature oscillations in loop heat pipe

operation, AIP Conference Proceedings. 255(2001) 255-262.

[17] J. Ku, Operating characteristics of loop heat pipes, in: 29st International Conference on Environmental Systems, 1999.

[18] H. Wang, G. Lin, X. Shen, L. Bai, D. Wen, Effect of evaporator tilt on a loop heat pipe with non-condensable gas, International Journal of Heat and Mass Transfer. 128(2019) 1072-1080.